Energy materials

NiP$_2$/FeP heterostructural nanoflowers interwoven by carbon nanotubes as highly efficient electrocatalyst for oxygen evolution reaction

Yanfang Liu[1], Bin Wang[2], Yingjiong Lu[2], Zhe Su[2], Yong Li[1], Qi Wu[1], Dongxu Yang[3,*], Yuanfu Chen[1,2,*] (iD), and Shifeng Wang[1,*]

[1] College of Science, and Institute of Oxygen Supply, Tibet University, Lhasa 850000, People's Republic of China

[2] State Key Laboratory of Electronic Thin Films and Integrated Devices, and School of Electronic Science and Engineering, University of Electronic Science and Technology of China, Chengdu 610054, People's Republic of China

[3] State Key Laboratory of Optical Technologies on Nano-Fabrication and Micro-Engineering, Institute of Optics and Electronics, Chinese Academy of Sciences, Chengdu 610209, People's Republic of China
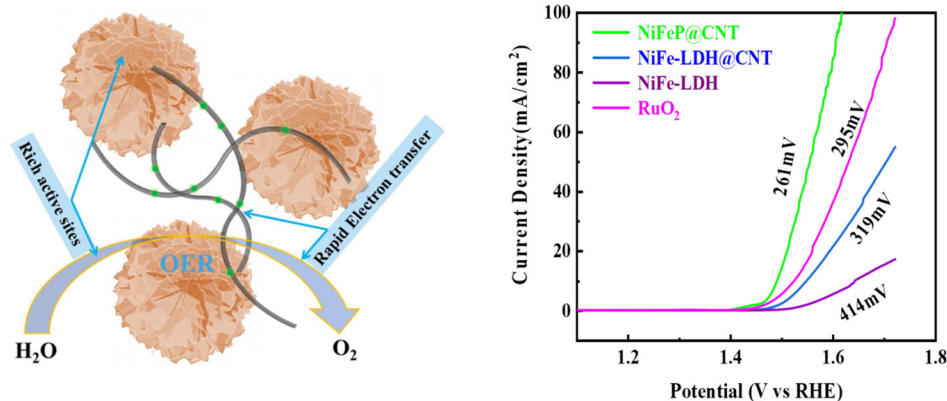
ABSTRACT

Oxygen evolution reaction (OER) for water splitting has a sluggish kinetics, thus significantly hindering the reaction efficiency. So far, it is still challenging to develop a cost-efficient and highly active catalyst for OER processes. To address such issues, we design and synthesize NiP$_2$/FeP heterostructural nanoflowers interwoven by carbon nanotubes (NiP$_2$/FeP@CNT) by a hydrothermal reaction followed by phosphating. The NiP$_2$/FeP@CNT catalyst delivers excellent OER performance: it displays an ultralow Tafel slope of 44.0 mV dec^{-1} and a relatively low overpotential of 261 mV at 10 mA cm^{-2}, better than RuO$_2$ commercial catalyst; it also shows excellent stability without observable decay after 20-h cycling. The outstanding OER property is mainly attributed to its special 3D stereochemical structure of CNT-interwoven NiP$_2$/FeP heterostructural nanoflowers, which is highly conductive and guarantees considerable active sites. Such nanostructure greatly facilitates the charge transfer, which significantly improves its electrocatalytic activity. This work offers a simple method to synthesize non-precious transition metal-based phosphide electrocatalysts with a unique hierarchical nanostructure for water splitting.

GRAPHICAL ABSTRACT

Introduction

The increasing energy consumption and the serious environmental pollution forces us to develop sustainable and environmentally friendly hydrogen energy [1–4]. Water splitting has attracted much attention as a green strategy for hydrogen energy production. However, the water-splitting efficiency is reduced by the slow dynamics of the multiple electron transfer in the oxygen evolution reaction (OER) process [5–9]. At present, RuO_2 or IrO_2 is still considered the mature catalyst in all respects, although the high price and scarcity hinder its large-scale applications [10–14]. Hence, it is urgent and essential to develop earth-abundant non-precious electrocatalysts for OER [15–17].

At present, great efforts have been made to explore non-noble metal catalyst materials, such as transition metal phosphates, sulfides, oxides, hydroxides and non-metallic catalysts [18–20]. Among various catalysts, transition metal phosphides have aroused the interest of many researchers because of their durable stability and remarkable OER performances [21]. In particular, NiFe-based phosphate is the most outstanding as a highly efficient catalyst for OER. Because the electronic interaction between Ni and Fe can regulate the affinity of the catalyst material surface to oxygen, so as to achieve the optimal conditions to promote the generation of oxygen molecules. At the same time, the morphology and structure of nanomaterials are also important factors to determine whether the performance is excellent. The catalyst materials with a three-diensonal structure increase the electrochemical surface area during the reaction. Therefore, it is very important to develop a three-dimensional transition metal phosphide catalyst [22].

Wang et al. [23] synthesized heterostructural nanoparticles growing on nanosheets which provide rich active surfaces, the overpotential (at $10\ mA\ cm^{-2}$) and the Tafel slope are 295 mV, and $59.1\ mV\ dec^{-1}$, respectively. Luo et al. [24] by hydrothermal method and phosphating prepared a novel nanostructure based on graphene oxide as a carrier, showing a small overpotential of 221 mV. However, the Tafel slope reached $105.7\ mV\ dec^{-1}$. Xuan et al. first synthesized Prussian blue analogues of NiFe, then phosphated its precursors, and finally produced the morphology of nanocube, which exposed more active sites. The overpotential was 271 mV ($10\ mA\ cm^{-2}$), and the corresponding Tafel slope was $53\ mV\ dec^{-1}$ [25]. The comparison of these reported studies shows that the transition metal phosphates have outstanding electrocatalytic activities for OER. However, the long-term stability of metal phosphides is still not so satisfactory compared to commercial RuO_2 or IrO_2 catalyst. Therefore, it is urgently desired to rationally design and facilely synthesize transition metal phosphide-based electrocatalysts with unique nanostructure and high efficiency for OER.

To address such issues, herein, NiP_2/FeP heterostructural nanoflowers interwoven by carbon nanotubes ($NiP_2/FeP@CNT$), are synthesized via a facile hydrothermal reaction followed with phosphating. The nanoflowers appear to unique 3D nanoporous architecture constructed by NiP_2/FeP heterostructural nanoflowers interwoven by highly conductive carbon nanotubes, this porous structure has good gas permeability and is conducive to the generation of oxygen. The $NiP_2/FeP@CNT$ catalyst delivers outstanding OER performance with a very low Tafel slope of 44.0 mV dec^{-1} and overpotential of 261 mV @ 10 mA cm^{-2} and excellent conductivity. This work provides a strategy for facile synthesis of catalysts with low cost, high conductivity and outstanding performance, which is promising for large-scale industrial application.

Experimental section

Synthesis of NiFe-LDH@CNT

NiFe-LDH@CNT was prepared via a one-pot solvothermal method. First, 1.2 g of CNT slurry was placed in a beaker containing 60 ml of deionized water and ultrasonized for 30 min. Precisely, 1 mmol of $Ni(NO_3)_2 \cdot 6H_2O$, 1 mmol of $Fe(NO_3)_3 \cdot 9H_2O$, 8 mmol NH_4F and 20 mmol of $CO(NH_2)_2$ were weighed and dissolved in the solution described above. The mixture was magnetically stirred for another 30 min. Then, after the mixture was evenly mixed, the mixture was transferred into 100 mL of the stainless steel Teflon-lined autoclave, and then heated to 120 °C for 12 h. After cooling down naturally, the obtained black product was washed several times with ethanol and DI water, then placed overnight in a vacuum freeze-dryer. At the end of the freeze-drying process, the sample is taken out and carefully ground into a powder for further use. For comparison, the synthesis of NiFe-LDH was identical to NiFe-LDH@CNT without the addition of CNT slurry.
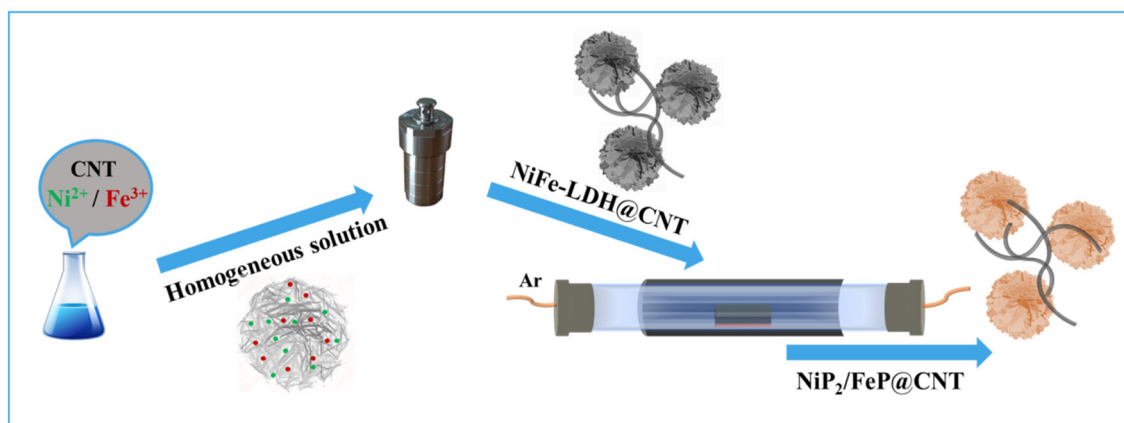
Synthesis of NiP₂/FeP@CNT nanoflowers

The as-prepared NiFe-LDH@CNT and $NaH_2PO_2 \cdot H_2O$ were placed in a tube furnace with two separate porcelain boats for annealing treatment under Ar atmosphere at 400 °C with temperature rising rate of

3 °C min^{-1} for 2 h. When the temperature of the tubular furnace naturally cools to the surrounding environment, the resulting product is named $NiP_2/FeP@CNT$. NiFeP is obtained in the same way, but the precursor is NiFe-LDH instead of NiFe-LDH@CNT.

Electrocatalytic measurements

The OER performances were performed on an electrochemical workstation (CHI660D) equipped with three electrodes in 1 M KOH solution at ambient temperature (298 K). Generally, a graphite rod was used as the counter electrode; and the Hg/HgO electrode was used as the reference electrode in OER; the glassy carbon electrode with the sample was used as a working electrode. The preparation method of the electrode is shown as follows. About 750 μL water and 250 μL ethanol were used to disperse 4 mg of the catalyst solid. Ultrasonication was performed for 10 min to evenly disperse the sample. Next, add 50 μL of 5 wt% Nafion solution to the above solution and continue ultrasonicated for a period of time. Finally, 5 μL of liquid was applied to the glass carbon electrode with a pipette gun and then dried in an oven at 60 °C for several minutes. In all measurements, potential values were changed to a reversible hydrogen electrode (RHE): $E_{RHE} = E_{Hg/HgO} + 0.923$ V. Before all electrochemical tests, an activation scan of minimum of 20 rounds of cyclic voltammetry (CV) cycles was performed at 100 mV s^{-1} to obtained stable curves. The linear sweep voltammetry of $NiP_2/FeP@CNT$ was tested at 1 mV s^{-1} to eliminate the redox peak, and the remaining samples were measured at 5 mV s^{-1}. And, the double-layer capacitance (C_{dl}) was also calculated from cyclic voltammogram (CV) data in 1 M KOH solution, which require sweeping rates from 20 to 200 mV s^{-1} over a range of potential tests, with a step of 20 mV s^{-1} for each curve. The electrochemical impedance spectroscopy (EIS) tests were performed from 100 kHz to 0.1 Hz. The long-time stability of $NiP_2/FeP@CNT$ was evaluated by continuous chronoamperometry using nickel foam (1 × 1 cm).

**Figure 1** Two-step fabrication process of NiP$_2$/FeP@CNT nanoflowers.

Results and discussion

The preparation of the NiP$_2$/FeP@CNT electrocatalyst is shown in the schematic diagram in Fig. 1, including a hydrothermal step followed by a phosphating reaction. Initially, the Teflon-lined autoclave with reactants was put in a hydrothermal oven for 12 h (120 °C) to get NiFe-LDH@CNT. Then, the appropriate amount of the above sample was placed together with sodium hypophosphite into a high-temperature tubular furnace at 400 °C for 2 h under continuous argon flow. After natural cooling to room temperature, the sample NiP$_2$/FeP@CNT was obtained.

The sample structure was performed by X-ray diffractions (XRD). As displayed in Fig. 2a, XRD patterns of NiFeP and NiP$_2$/FeP@CNT shows characteristic peaks at 31.6°, 35.9°, 40.7°, 47.9° and 55.4°, corresponding to the (200), (210), (211), (220) and (311) planes of NiP$_2$, respectively.

The other signals at 32.7°, 37.2° and 48.3°can be attributed to the (011), (111), (211) planes of FeP, respectively [23, 24]. Then, the Raman spectrum of the NiP$_2$/FeP@CNT is provided, considering the signal of carbon can not be detected by XRD characterization. As shown in Fig. 2b, characteristic Raman peaks can be clearly seen at 1350 cm^{-1} and ~1600 cm^{-1}, which can be assigned to the D, and G bands of carbon nanotubes, respectively [25]. In order to get the information of the surface properties of NiP$_2$/FeP@CNT, the BET test was acquired through N$_2$ adsorption–desorption-isotherm as displayed in Fig. 2c, d. The NiP$_2$/FeP@CNT shows a BET surface area of 68.36 m^2 g^{-1}, considerably larger than that of NiFeP (23.07 m^2 g^{-1}) [26, 27]. Additionally, The

distribution of pore size obtained from the Barrett–Joyner–Halenda (BJH) method is presented in Fig. 2d. The NiP$_2$/FeP@CNT displays great probabilities at the range of 20–60 nm, confirming the overwhelming existence of mesopores, which is rarely observed in the sample NiFeP. The larger surface area and higher mesoporous percentage are the result of the specific microtopography of nanoflower as well the carbon nanotube networks. More importantly, from a microstructure point of view, the larger surface area and higher mesoporous percentage are generally favored in catalysis due to the greatly increase in active sites and facilitate mass transfer [20].

X-ray photoelectron spectroscopy (XPS) analysis was performed for NiP$_2$/FeP@CNT. As shown in Fig. S2 and Fig. 3, the XPS survey spectrum of NiP$_2$/FeP@CNT shows the coexistence of Fe, Ni C, P and O. The XPS spectrum of C 1 s in Fig. 3a exhibits three peaks at 289.7, 285.0 and 283.8 eV, which corresponds to O–C = O, C–O and C–C bonds, respectively [23, 26]. The XPS spectrum of Fe 2p is shown in Fig. 3b. It can be observed that there are two peaks at 706.5 and 724.1 eV, matching with the Fe 2p$_{3/2}$ and Fe 2p$_{1/2}$ of FeP, respectively. The wider peak at 710.0 eV and 713.3 eV are ascribed to the oxidation peak of Fe and shakeup satellite. Figure 3c shows the XPS spectrum of Ni 2p. There are three peaks at 853.6, 856.1 and 860.4 eV, corresponding to Ni^{2+}, Ni^{3+} and the satellite peaks of Ni 2p$_{3/2}$, respectively. Ni^{2+}, Ni^{3+} and the satellite peaks in Ni 2p$_{1/2}$ are located at 870.4, 874.3 and 879.1, respectively [28]. In P 2p spectrum, as shown in Fig. 3d, the characteristic signal of P 2p$_{3/2}$ and P 2p$_{1/2}$ with peaks at 128.8 and 129.6 eV reflect the formation of phosphide, and the
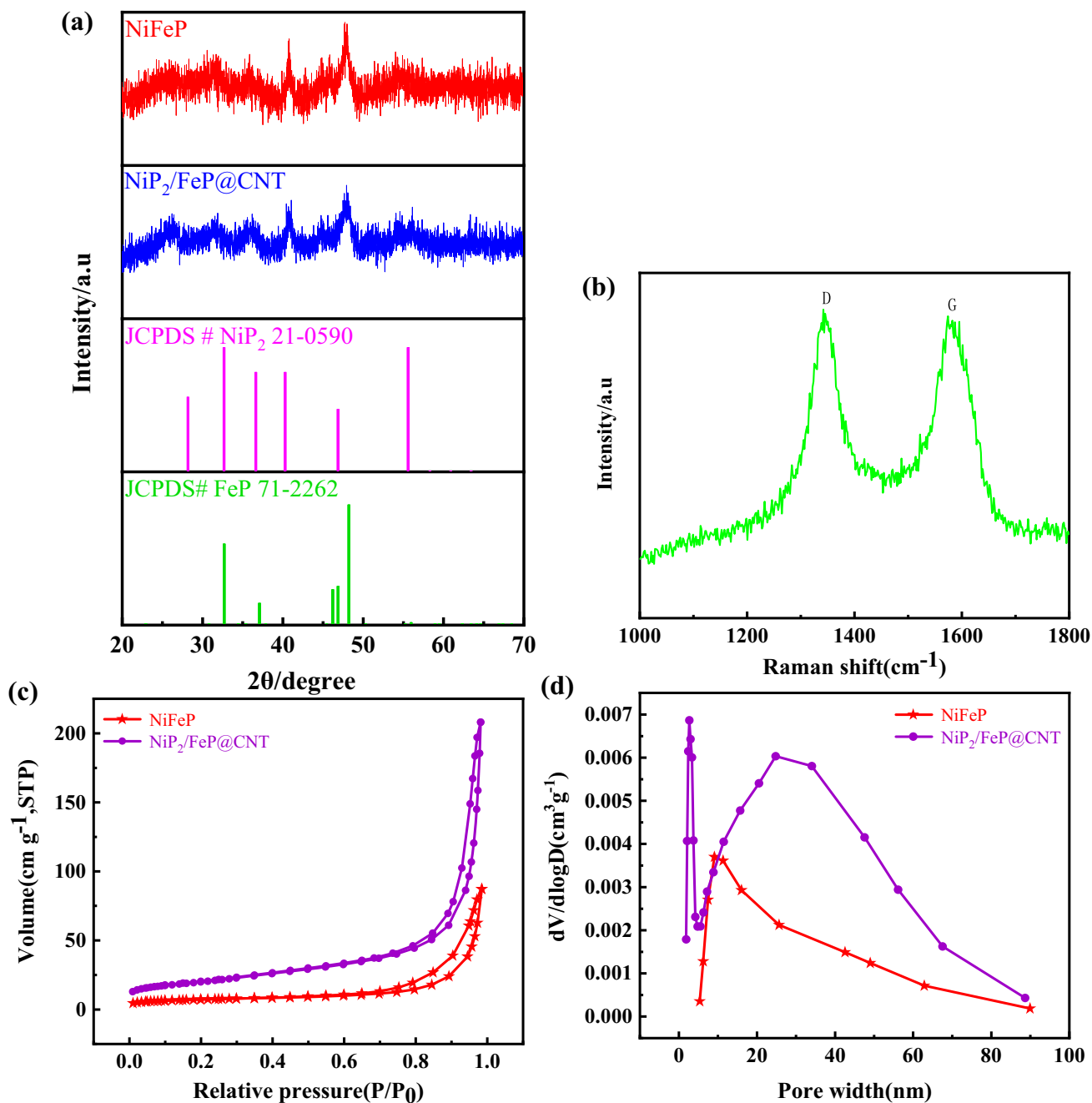
Figure 2 **a** XRD patterns of NiFeP and $NiP_2/FeP@CNT$. **b** Raman spectrum of $NiP_2/FeP@CNT$. **c** N_2 adsorption/desorption isotherms, and **d** pore-size distribution plots of NiFeP and $NiP_2/FeP@CNT$.

other peak at 133.8 eV belong to the P–O band [26, 31].

The morphologies of the samples can be clearly revealed by scanning electron microscopy (SEM) and transmission electron microscopy (TEM). As shown in Fig. 4a, $NiP_2/FeP@CNT$ shows the morphology of nanoflowers supported by a network of carbon nanotubes, which is similar to the structure of neural

networks in the human body [25]. In Fig. S1a, b, the obtained NiFe-LDH@CNT presents as homogeneous nanoflowers dispersed in the CNT network. After the phosphating treatment, these nanoflowers were tightly wrapped with carbon nanotubes, with the size and shape well maintained (Fig. 4a). The SEM images of the other reference samples are displayed in Fig. S1. In Fig S1. a and b, we can clearly see the
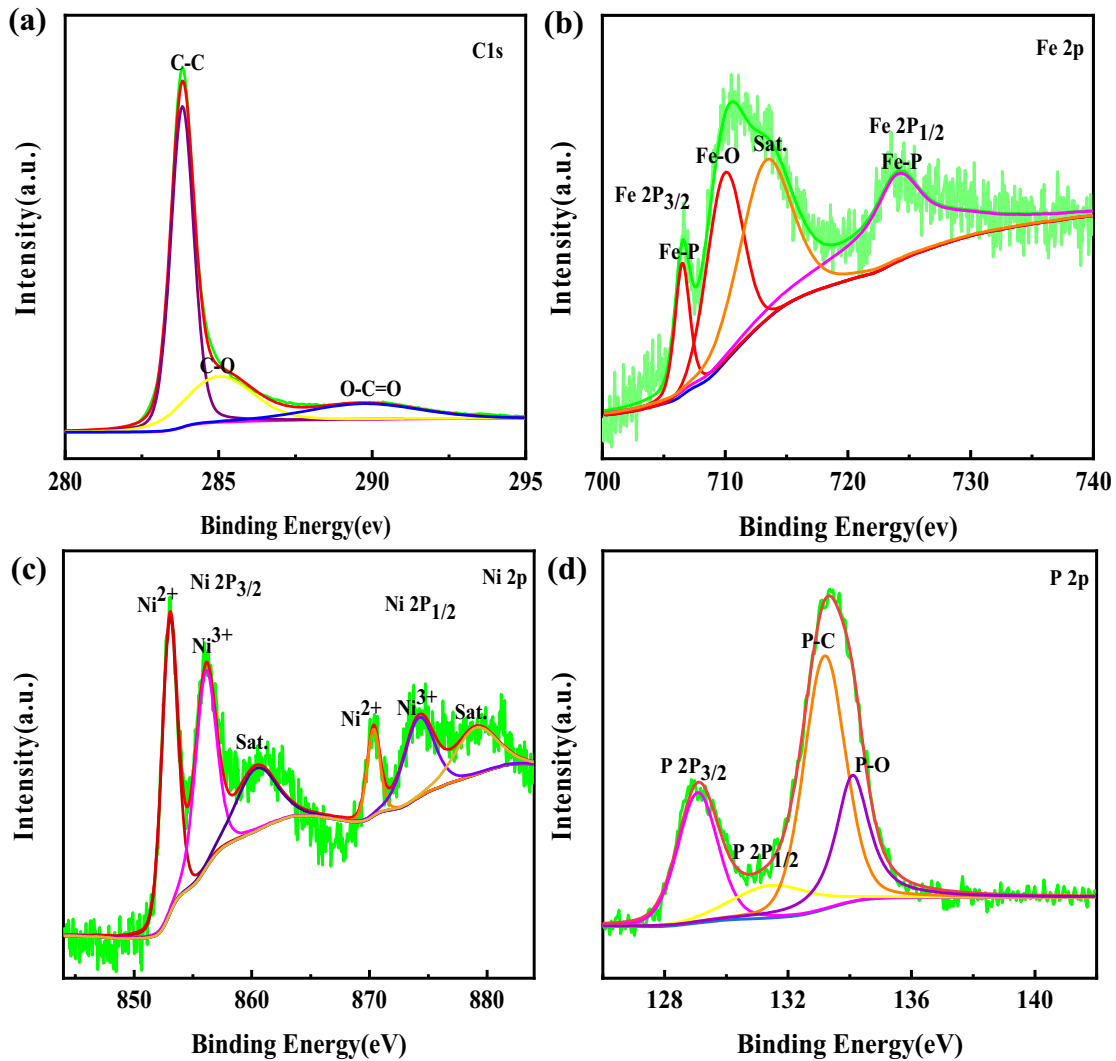
Figure 3 **a** C 1s, **b** Fe 2p, **c** Ni 2p and **d** P 2p XPS spectra of NiP$_2$/FeP@CNT.

interweaving of nanoflowers and carbon nanotubes, which proves that the morphology of the sample remains the same after phosphating. Meanwhile, this is also confirmed by the TEM image (Fig. 4b). High-resolution TEM (HRTEM) image of NiP$_2$/FeP@CNT (Fig. 4c, d) shows lattice spacing of 0.188 and 0.219 nm, which are consistent with the plane (211) of FeP and (211) of NiP$_2$. The EDX spectrum and the content of the element can prove the existence of C, P, Ni and Fe elements (Fig. S4, Table S1). From the element mapping images (Fig. 4e–i), it can be further concluded that these elements are evenly distributed in the sample.

Considering the nanoflower morphology of NiP$_2$/FeP@CNT, good catalytic performance is expected. The OER electrochemical activity of NiP$_2$/FeP@CNT

was evaluated in a conventional three-electrode setup in alkaline electrolyte. Figure 5a shows the linear sweep voltammetry (LSV) plots of NiP$_2$/FeP@CNT, NiFeP, NiFe-LDH@CNT, NiFe-LDH and RuO$_2$. NiP$_2$/FeP@CNT needs 261 mV to deliver 10 mA cm^{-2}, while NiFeP, NiFe-LDH@CNT, NiFe-LDH and RuO$_2$ require 319, 319, 414 and 295 mV, respectively. Compared NiFe-LDH@CNT, the performance of NiP$_2$/FeP@CNT is greatly improved, which proves that phosphating plays a very significant role. Figure 5b shows the Tafel slopes of NiP$_2$/FeP@CNT, NiFeP, NiFe-LDH@CNT, NiFe-LDH and RuO$_2$. Besides, NiP$_2$/FeP@CNT delivers the lowest Tafel slope of is 44 mV dec^{-1}. The order of Tafel slope is NiP$_2$/FeP@CNT (44 mV dec^{-1}) < NiFe-LDH@CNT (62 mV dec^{-1}) < NiFeP(68 mV dec^{-1}) < RuO$_2$
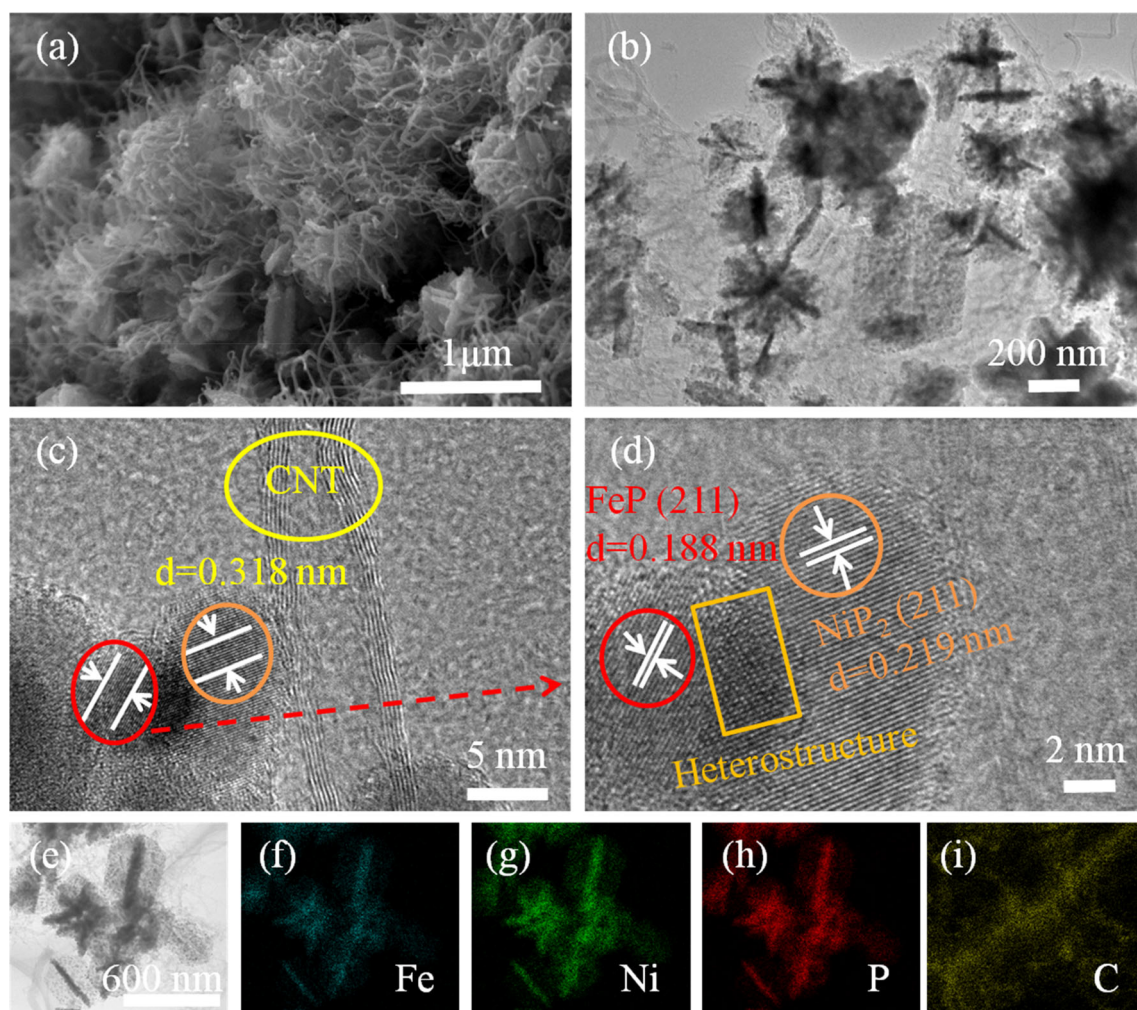
Figure 4 **a** SEM image, **b** TEM image, **c-d** HRTEM images. **d** The magnified image of the square frame mark in (**c**). **e** Morphology and **f-i** corresponding elemental mapping images of $NiP_2/FeP@CNT$.

$(73 \text{ mV dec}^{-1}) < \text{NiFe-LDH} (76 \text{ mV dec}^{-1})$. Obviously, $NiP_2/FeP@CNT$ shows the best OER activity, making this unique 3D nanoflower interwoven by carbon network as an excellent non-noble metal-based OER catalyst material [23, 29, 30].

Electrochemical active surface area (ECSA) is a key factor of catalyst property, which is usually characterized by the double-layer capacitance (C_{dl}). The C_{dl} was obtained by performing CV scans with different rates over a certain voltage range (Fig. S3). Notably, the C_{dl} values of $NiP_2/FeP@CNT$ and NiFe-LDH@CNT are very similar, which is consistent with the similar morphology between the two materials. This result indicates that the optimal performance of $NiP_2/FeP@CNT$ is attributed to an enhanced catalytic activity instead of the surface area change.

Electrochemical impedance spectroscopy (EIS) was usually used to characterize the charge transfer status during the OER process. The obtained Nyquist plots are shown in Fig. 5d. $NiP_2/FeP@CNT$ has the smallest charge transfer resistance (R_{ct}), indicating a smooth charge transfer and thus a rapid reaction.

The mechanism for the high performance of $NiP_2/FeP@CNT$ can be summarized as below. First of all, the addition of carbon nanotube networks improved the electrical conductivity of the material. Secondly, the three-dimensional structure of the nanoflower structure exposed more active areas and active sites. Finally, the presence of heterojunctions offers a strong synergistic effect, which further enhances the catalytic activity.
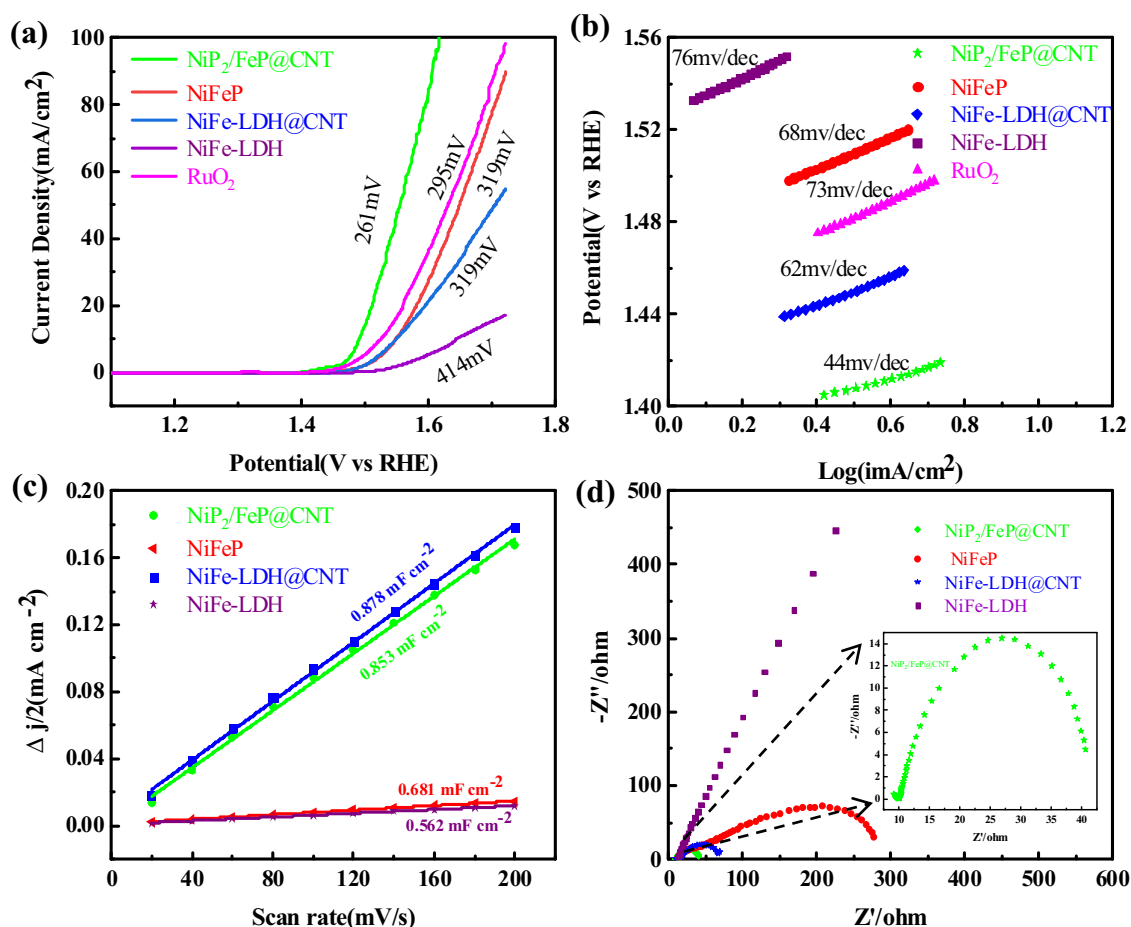
Figure 5 a LSV curves in 1 M KOH solution and **b** corresponding Tafel plots of NiP$_2$/FeP@CNT, NiFeP, NiFe-LDH@CNT, NiFe-LDH and RuO$_2$. **c** Estimated C$_{dl}$ values and relative electrochemically active surface areas, and **d** Nyquist plots of NiP$_2$/FeP@CNT, NiFeP, NiFe-LDH@CNT and NiFe-LDH. The inset of (d) is the magnification of the EIS spectrum of NiP$_2$/FeP@CNT.

In addition, enduring stability is another important factor in evaluating the performance of catalyst materials. As shown in Fig. 6b, the current density maintained almost unchanged during the 20 h test. The disadvantage is that a higher voltage is displayed after 3000 cycles. Despite this, NiP$_2$/FeP@CNT still has great prospects for OER in alkaline media [32].

Conclusion

In summary, NiP$_2$/FeP@CNT heterostructural nanoflowers interwoven by carbon nanotubes are synthesized by the strategy of hydrothermal and subsequent phosphating. The NiP$_2$/FeP@CNT hybrid shows an ultralow overpotential (261 mV) to deliver 10 mA cm^{-2} and a small Tafel slope (44 mV dec^{-1}). The outstanding properties are assigned to the 3D structure of CNT-interwoven NiP$_2$/FeP heterostructural nanoflowers, which provides rich active sites and enhanced conductivity. Significantly, the synergistic effect between the ultrathin NiP$_2$/FeP heterostructural flowers and the skeleton carbon nanotubes favors charge transfer and ion diffusion. This work offers a simple method to synthesize non-precious transition metal-based phosphide electro-catalysts with a unique hierarchical nanostructure for water splitting.

(a)

(b)
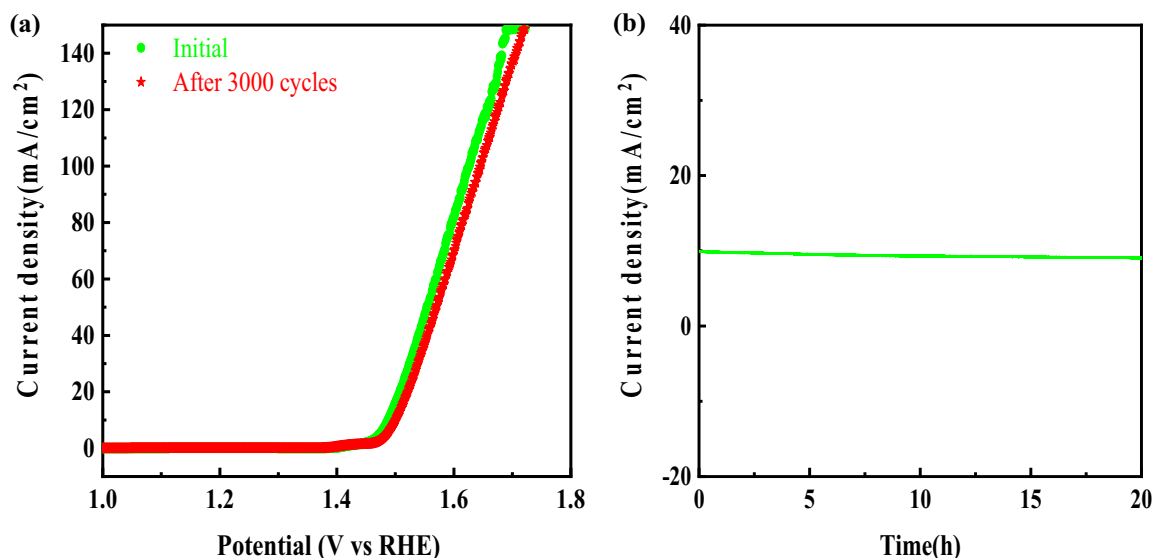
Figure 6 **a** CV performance of NiP$_2$/FeP@CNT toward OER. **b** Chronopotentiometric curves of NiP$_2$/FeP@CNT with the current density of 10 mA cm^{-2} in 1 M KOH solution.

Declaration

Conflict of interest There are no conflicts of interests.

References

[1] Huo D, Song F, Hu J, Yuan J, Niu L, Wang A-j (2021) One-step synthesis of carbon-encapsulated nickel phosphide nanoparticles with efficient bifunctional catalysis on oxygen evolution and reduction. Int J Hydrog Energy 46(12):8519–8530

[2] Li D, Liu C, Ma W et al (2021) Fe-doped NiCoP/prussian blue analog hollow nanocubes as an efficient electrocatalyst for oxygen evolution reaction. Electrochim Acta 367:137492

[3] Li Y, Ge L, Zhou Y et al (2020) KB-templated in situ synthesis of highly dispersed bimetallic NiFe phosphides as efficient oxygen evolution catalysts. Inorg Chem Front 7(24):4930–4938

[4] Lim D, Lim C, Hwang M, Kim M, Shim SE, Baeck S-H (2021) Facile synthesis of flower-like P-doped nickel-iron disulfide microspheres as advanced electrocatalysts for the oxygen evolution reaction. J Pow Sour 490:229552

[5] Xu H, Ye K, Zhu K et al (2020) Transforming carnation-shaped MOF-Ni to Ni–Fe prussian blue analogue derived efficient bifunctional electrocatalyst for urea electrolysis. ACS Sustain Chem Eng 8(42):16037–16045

[6] Cui Z, Lin J, Wu J, Yu J, Si J, Wang Q (2021) N- doped CoP nanoparticles embedded in electrospun N-doped porous carbon nanofiber as high-efficiency oxygen evolution electrocatalysts. J Alloys Compd 854:156830

[7] Fei L, Sun H, Ran R, Zhou W, Shao Z (2021) Self-supported nickel phosphide electrode for efficient alkaline water-to-hydrogen conversion via urea electrolysis. Ind Eng Chem Res 60(3):1185–1193

[8] Wang C, Shang H, Xu H, Du Y (2021) Nanoboxes endow non-noble-metal-based electrocatalysts with high efficiency for overall water splitting. J Mater Chem A 9(2):857–874

[9] Chen D, Chen Y, Zhang W, Cao R (2021) Nickel selenide from single-molecule electrodeposition for efficient electrocatalytic overall water splitting. New J Chem 45(1):351–357

[10] Yu J, Cheng G, Luo W (2017) Hierarchical NiFeP microflowers directly grown on Ni foam for efficient electrocatalytic oxygen evolution. J Mater Chem A 5(22):11229–11235

[11] Wang J, Chen C, Cai N, Wang M, Li H, Yu F (2021) High topological tri-metal phosphide of CoP@FeNiP toward

enhanced activities in oxygen evolution reaction. Nanoscale 13(2):1354–1363

[12] Wei B, Xu G, Hei J, Zhang L, Huang T (2021) PBA derived FeCoP nanoparticles decorated on NCNFs as efficient electrocatalyst for water splitting. Int J Hydrog Energy 46(2):2225–2235

[13] Anantharaj S, Sugime H, Chen B, Akagi N, Noda S (2020) Boosting the oxygen evolution activity of copper foam containing trace Ni by intentionally supplementing Fe and forming nanowires in anodization. Electrochim Acta 364:137170

[14] Wu X, Li J, Li Y, Wen Z (2021) NiFeP-MoO$_2$ hybrid nanorods on nickel foam as high-activity and high-stability electrode for overall water splitting. Chem Eng J 409:128161

[15] Tong J, Li C, Bo L et al (2021) Bimetallic Fe–Co chalcogenophosphates as highly efficient bifunctional electrocatalysts for overall water splitting. Int J Hydrog Energy 46(5):3354–3364

[16] Kang Y, Wang S, Zhu S et al (2021) Iron-modulated nickel cobalt phosphide embedded in carbon to boost power density of hybrid sodium–air battery. Appl Catal B Environ 285:119786

[17] Liu X, Yao Y, Zhang H et al (2020) In situ-grown cobalt-iron phosphide-based integrated electrode for long-term water splitting under a large current density at the industrial electrolysis temperature. ACS Sustain Chem Eng 8(48):17828–17838

[18] Suryawanshi UP, Ghorpade UV, Lee DM et al (2020) Colloidal Ni$_2$P nanocrystals encapsulated in heteroatom-doped graphene nanosheets: a synergy of 0D@2D heterostructure toward overall water splitting. Chem Mater 33(1):234–245

[19] Shuai C, Mo Z, Niu X et al (2020) Nickel/cobalt bimetallic phosphides derived metal-organic frameworks as bifunctional electrocatalyst for oxygen and hydrogen evolution reaction. J Alloys Compd 847:156514

[20] Wang B, Chen Y, Wang X et al (2020) A microwave-assisted bubble bursting strategy to grow Co$_8$FeS$_8$/CoS heterostructure on rearranged carbon nanotubes as efficient electrocatalyst for oxygen evolution reaction. J Pow Sour 449:227561

[21] Wang Y, Sun L, Lu L, Xu D, Hao Q, Liu B (2021) A sequential template strategy toward hierarchical hetero-metal phosphide hollow nanoboxes for electrocatalytic oxygen evolution. J Mater Chem A 9(6):3482–3491

[22] Wang Z, Wei C, Zhu X, Wang X, He J, Zhao Y (2021) A hierarchical carbon nanotube forest supported metal phosphide electrode for efficient overall water splitting. J Mater Chem A 9(2):1150–1158

[23] Wang H, Wang X, Zheng B, Yang D, Zhang W, Chen Y (2019) Self-assembled Ni$_2$P/FeP heterostructural

nanoparticles embedded in N-doped graphene nanosheets as highly efficient and stable multifunctional electrocatalyst for water splitting. Electrochim Acta 318:449–459

[24] Luo S, Wang R, Hei P, Gao L, Yang J, Jiao T (2021) Self-assembled Ni$_2$P nanosheet-implanted reduced graphene oxide composite as highly efficient electrocatalyst for oxygen evolution reaction. Coll Surf A Physicochem Eng Asp 612:125992

[25] Wang B, Hu Y, Yu B, Zhang X, Yang D, Chen Y (2019) Heterogeneous CoFe–Co$_8$FeS$_8$ nanoparticles embedded in CNT networks as highly efficient and stable electrocatalysts for oxygen evolution reaction. J Pow Sour 433:126688

[26] Li W, Chen Y, Yu B, Hu Y, Wang X, Yang D (2019) 3D hollow Co–Fe–P nanoframes immobilized on N, P-doped CNT as an efficient electrocatalyst for overall water splitting. Nanoscale 11(36):17031–17040

[27] Wu Y, Xiao Z, Jin Z, Li X, Chen Y (2021) The cobalt carbide/bimetallic CoFe phosphide dispersed on carbon nanospheres as advanced bifunctional electrocatalysts for the ORR, OER, and rechargeable Zn-air batteries. J Coll Interface Sci 590:321–329

[28] Song C, Liu Y, Wang Y, Tang S, Li W, Li Q, Zeng J, Chen L, Peng H, Lei Y (2021) Highly efficient oxygen evolution and stable water splitting by coupling NiFe LDH with metal phosphides. Sci China Mater 64(7):1662–1670

[29] Wu Y, Li Y, Yuan M, Lü Z, Xu L, Wei B (2020) Direct growth of Ni–Fe phosphides nanohybrids on NiFe foam for highly efficient water oxidation. J Alloys Compd 847:156363

[30] Liu H, Zhu S, Cui Z, Li Z, Wu S, Liang Y (2021) Ni$_2$P nanoflakes for the high-performing urea oxidation reaction: linking active sites to a UOR mechanism. Nanoscale 13(3):1759–1769

[31] Wang B, Chen Y, Wang X, Ramkumar J, Zhang X, Yu B, Yang D, Karpuraranjith M, Zhang W (2020) rGO wrapped trimetallic sulfide nanowires as an efficient bifunctional catalyst for electrocatalytic oxygen evolution and photocatalytic organic degradation. J Mater Chem A 8:13558–13571

[32] Wang B, Chen Y, Wu Q, Lu Y, Zhang X, Wang X, Yu B, Yang D, Zhang W (2021) A co-coordination strategy to realize janus-type bimetallic phosphide as highly efficient and durable bifunctional catalyst for water splitting. J Mater Sci Technol 74:11–20. https://doi.org/10.1016/j.jmst.2020.10.009